# Multicore optical fiber shape sensors suitable for use under gamma radiation

DAVID BARRERA,[1,*] ID JAVIER MADRIGAL,[2] ID SYLVIE DELEPINE-LESOILLE,[3] AND SALVADOR SALES[2] ID

[1]*Dept. of Electronics, University of Alcalá, Edificio Politécnico Superior, 28805 Alcalá de Henares, Spain*
[2]*ITEAM Research Institute, Universitat Politècnica de València, camino de Vera s/n 46022, Spain*
[3]*Andra, 1-7 rue Jean Monnet, 92298 Chatenay-Malabry, France*
*[*]david.barrera@uah.es*

**Abstract:** We have designed and implemented a fiber optic shape sensor for high-energy ionizing environments based on multicore optical fibers. We inscribed two fiber Bragg gratings arrays in a seven-core optical fiber. One of the arrays has been inscribed in a hydrogen-loaded fiber and the other one in an unloaded fiber in order to have two samples with very different radiation sensitivity. The two samples were coiled in a metallic circular structure and were exposed to gamma radiation. We have analyzed the permanent radiation effects. The radiation-induced Bragg wavelength shift (RI-BWS) in the hydrogen-loaded fiber is near ten times higher than the one observed for the unloaded fiber, with a maximum wavelength shift of 415 pm. However, the use of the multiple cores permits to make these sensors immune to RI-BWS obtaining a similar curvature error in both samples of approximately 1 cm without modifying the composition of the fiber, pre-irradiation or thermal treatment.

## 1. Introduction

Optical fiber sensors (OFSs) have multiple advantages that make them excellent candidates for their use in extreme environmental conditions. They are immune to electromagnetic interferences, have a negligible ignition risk, can be designed to withstand high temperatures and are chemically inert. Additionally, OFSs offer the possibility to multiplex sensors in the same optical fiber or make truly distributed measurements. All these properties have attracted the attention of different research groups to study the performance of these sensors in harsh environments like high temperatures, high pressures or high-energy ionizing environments [1–4]. High-energy ionizing environments are particularly demanding even for optical fibers and OFSs. The effects of radiation over the optical fibers have been studied in the past. The main effects of radiation on optical fibers are radiation-induced emission (RIE), radiation-induced attenuation (RIA) and radiation-induced refractive index change (RIRIC) [5]. The RIE is a luminescence emission that is guided by the optical fiber and its effects are more important at visible wavelengths. Radiation-induced attenuation (RIA) is an increment of the optical fiber losses that it is induced when it is irradiated. RIA affects all the OFS and can reduce the maximum length of OFS. Although this attenuation is partially recovered after the irradiation, the RIA is an important limitation especially for amplitude-based–OFS. Radiation-hardened fibers have been developed to minimize the RIA but it does not exist an ideal composition of these fibers due to the numerous parameters that influence the sensitivity to radiation [6,7]. Whereas RIA can reduce the signal to noise ratio, the RIRIC modifies the refractive index of the optical fiber depending on the radiation conditions and the optical fiber composition. This effect can be a strong limitation for OFSs that use the wavelength as a reference, like fiber Bragg grating (FBG) sensors, limiting their accuracy. In FBG sensors, the change of the Bragg wavelength due to radiation effects is normally referred to as radiation-induced Bragg wavelength shift (RI-BWS). Several studies have explored the use of FBGs under radiation and tried to identify the best fiber composition,

inscription conditions and previous or posterior thermal treatments to reduce the wavelength shift due to radiation [4–11]. All these efforts have limited the maximum RI-BWS. A. Morana et al. obtained a maximum RI-BWS lower than 10 pm and more recently J. Kuhnhenn et al. obtained a RI-BWS in the order of 2 pm. In both cases a correct thermal treatment is needed after the FBG inscription [9,10].

We propose to use a differential wavelength shift measurement scheme to implement sensors for high-energy ionizing environments. In this scheme, two or more FBGs are needed. The FBGs are exposed to the same irradiation conditions and the radiation effect in these FBGs are the same. However, we modify the FBGs sensitivities to the parameter we want to measure, i.e. curvature, strain or temperature, to encode the sensor output. This hardened by design architecture can be done in a more convenient way using multicore optical fibers (MCF) where the radiation conditions are similar in all the cores and the FBGs sensitivity can be modified bending the fiber [12].

MCFs have been used to implement curvature and shape sensors [13,14]. In these sensors, the FBGs inscribed in the cores of an MCF have different sensitivities depending on the relative position of the cores inside the optical fiber and the curvature direction. The curvature magnitude and direction are determined using the differences between the wavelength shifts of the FBGs. The same principle can be used to implement sensors for different parameters.

In this paper, we have inscribed two arrays of FBGs in all the cores of a seven-core MCF, one in a hydrogen-loaded fiber and one more in a non-hydrogen-loaded fiber to intentionally have samples with different radiation sensitivities. The two arrays were coiled in a metallic circular structure to maintain the shape through the experiment and then, they were irradiated. We have analyzed the permanent effects of $\gamma$-radiation in order to demonstrate the compatibility of this measurement scheme under high-energy ionizing environments. To the best of our knowledge, this is the first proposed optical sensor based on multicore optical fibers for radiation environments. Our main objective is to demonstrate that multicore optical fiber sensors can be used under gamma radiation without modifying their composition or the need of additional treatments. The same principles described in this paper can be applied to design other sensors.

## 2. Sensor fabrication

We have used a seven-core MCF (SM-7C1500) manufactured by Fibercore Ltd. The cores of the MCF are doped with germanium and are placed in a hexagonal pattern with a core spacing of 35 µm. We prepared two samples of this fiber. One of the samples was introduced in a hydrogen chamber for 14 days at a pressure of 50 bar and ambient temperature to increase the photosensitivity. The other sample remained unloaded. After the hydrogen-loading process, we removed the acrylic coating and inscribed an array of four type I FBGs in both samples. The inscription was made simultaneously in all the cores giving a total of 28 FBGs in each sample (see Fig. 1).
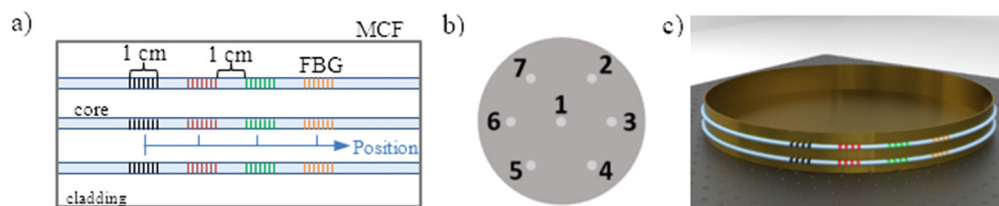


**Fig. 1.** (a) Description of the FBG array. (b) Core number scheme. (c) Drawing of the metallic support with the two FBG arrays coiled.

We used a CW frequency-doubled argon-ion laser at 244 nm and a moving phase/fiber technique. The inscribed FBGs are 10 mm long with a 10 mm spacing between them. No additional thermal treatments were performed to the fibers and the coating was not replaced in order to not influence the radiation sensitivity of the FBGs [15].

We consecutively measured the reflected and transmitted optical spectrum of the FBG array in all the fiber cores for both samples using four fan-in/out devices (two per sample) and a Yenista TS100HP tunable laser with a Yenista CT400 component analyzer. Figure 2 shows the obtained spectra. The reflectivity of the FBGs inscribed in the unloaded fiber is lower than the ones inscribed in the hydrogen-loaded sample.
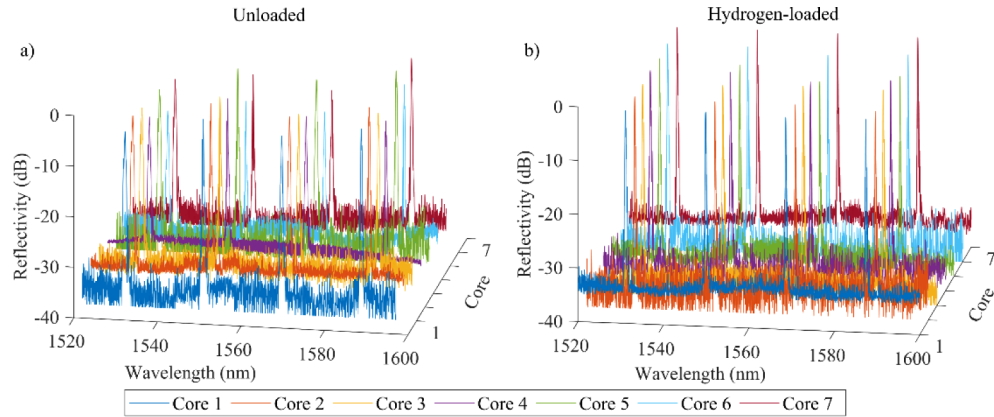


**Fig. 2.** FBG array spectrum in the central core. (a) Unloaded fiber. (b) Hydrogen-loaded fiber

The two arrays were coiled and mechanically attached to a circular-shape metallic structure with a diameter of 20 cm to maintain the shape through all the experiment. The optical spectra of the FBGs were measured after coiling the two samples. Finally, the fan-in/outs were then removed to prevent their irradiation.

## 3. Irradiation

The sample irradiation was performed at IRMA facilities, France, one month after the hydrogen loading. The metallic support with the FBG arrays coiled was placed in the irradiation chamber at a distance of 65.8 cm from a $^{60}$Co source, which consists of 4 rods, reaching a total activity of 916.02 TBq. It was placed vertically to ensure that all the gratings receive the same dose rate.

The sample was irradiated for 13 days and 18 hours, with a dose rate of about 58Gy/h, up to a total dose of about 192 kGy. Figure 3 describes the irradiation chamber and the relative position of the FBG arrays and the $^{60}$Co source.
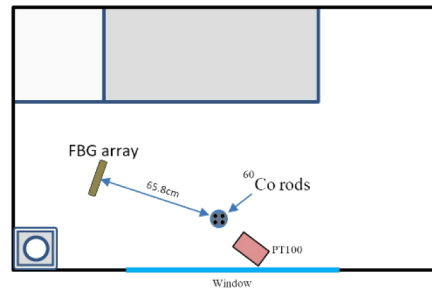
**Fig. 3.** Description of the sensor location inside the irradiation chamber.

## 4. Experimental results

Six weeks after the exposure we spliced again the two samples to the fan-in/out devices. The two samples remained attached to the metallic support after the irradiation in order to compare the results before and after the irradiation. We analyze the permanent effects of $\gamma$-irradiation.

Figures 4 and 5 compare the optical spectra of the FBGs in a straight position (blue), coiled in the metallic support (red), and coiled after the irradiation (green). Figure 4 shows the spectra of two cores at opposite sides of the fiber in the unloaded sample. Core #3 is on the inner side of the curvature and shows a wavelength shift towards the blue whereas core #6 is on the external side of the curvature. Comparing the optical spectra before and after the irradiation, the FBG spectra show a small reduction of their reflectivity and a small wavelength shift. The two measurements were taken approximately at the same room temperature ($\pm 0.5°C$). The mean wavelength shift of all the FBGs is 27 pm. Taking into account the temperature sensitivity of 9.8pm/°C of the FBGs we have an uncertainty of $\pm 4.9$ pm. The mean signal-to-noise ratio is reduced by 0.63 dB.
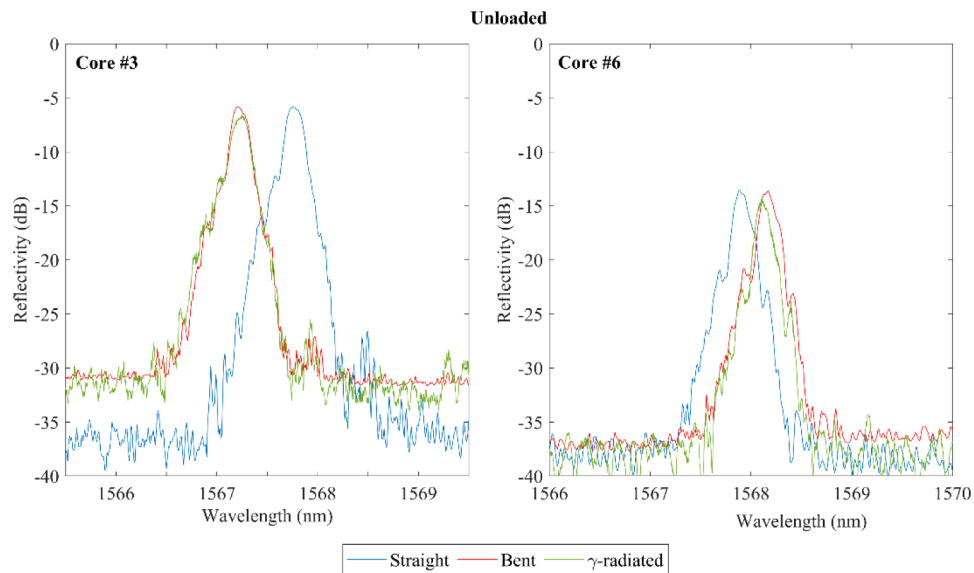


**Fig. 4.** FBG spectra at straight position, after coiling and after $\gamma$-irradiation in the unloaded sample. Core #3 is in the inner side of curvature whereas core #5 is in the external side.

Figure 5 shows the results for the hydrogen-loaded sample. In this sample, core #5 is on the inner side of the curvature and core #2 is on the external side. After the irradiation, the FBG
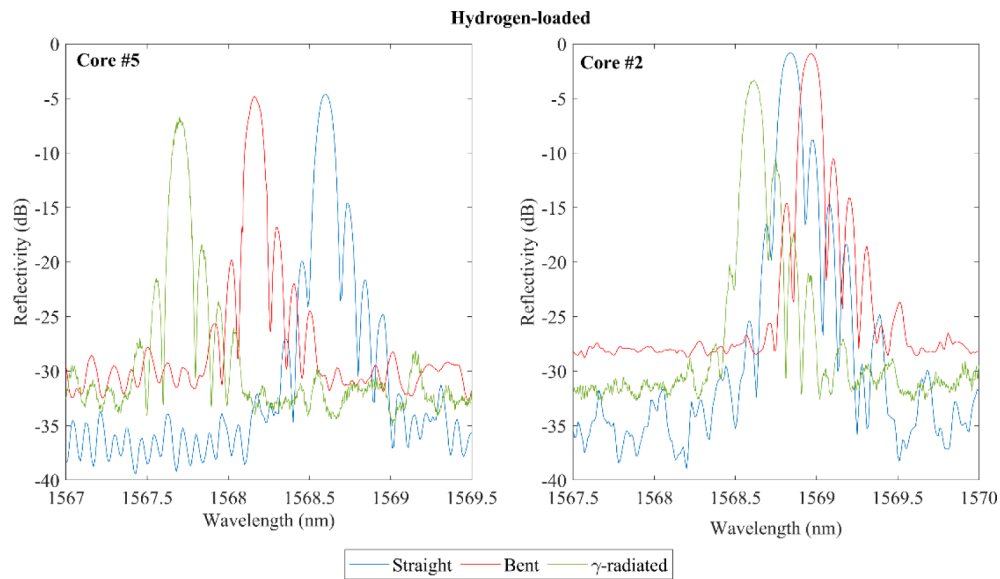
**Fig. 5.** FBG spectra at straight position, after coiling and after $\gamma$-irradiation in the hydrogen-loaded sample. Core #5 is in the inner side of curvature whereas core #2 is in the external side.

reflectivity decreases with a mean signal-to-noise ratio reduced by 2.21 dB. In the hydrogen-loaded fiber, the FBG spectra show a higher wavelength shift compared with the one obtained for the unloaded fiber. The mean wavelength shift in the hydrogen-loaded fiber is 345 pm, with a maximum wavelength shift of 415 pm, more than ten times greater than the wavelength shift observed in the unloaded fiber.

These results are in agreement with previous studies in single-core non-radiation-hardened fibers with and without hydrogen loading [4–11].

Table 1 and Table 2 summarizes the measured FBG wavelength before and after $\gamma$-irradiation. Column labeled as B indicates the wavelength shift after bending the fiber in the metallic support and column labeled as I the additional wavelength shift after the irradiation of the fiber. Note that the initial FBG wavelength is measured under a small strain to maintain the fiber straight that is removed when the fiber is coiled. The Bragg wavelength have been determined using a second order polynomial fitting [16].

**Table 1. Unloaded sample. Initial FBG wavelength (straight) and wavelength shifts (in pm) after bending (B) and after irradiation (I)**

|      | FBG 1    |      |     | FBG 2    |      |     | FBG 3    |      |     | FBG 4    |      |     |
|------|----------|------|-----|----------|------|-----|----------|------|-----|----------|------|-----|
| Core | Initial  | B    | I   | Initial  | B    | I   | Initial  | B    | I   | Initial  | B    | I   |
| 1    | 1530.218 | −143 | 6   | 1548.919 | −145 | 8   | 1567.731 | −148 | 18  | 1586.796 | −141 | 16  |
| 2    | 1530.058 | −409 | 49  | 1548.755 | −418 | 16  | 1567.576 | −467 | 39  | 1586.667 | −498 | 8   |
| 3    | 1530.230 | −518 | −12 | 1548.940 | −526 | −18 | 1567.762 | −555 | 43  | 1586.818 | −501 | −23 |
| 4    | 1530.033 | −253 | −65 | 1548.730 | −256 | −36 | 1567.539 | −240 | 13  | 1586.597 | −158 | −9  |
| 5    | 1530.417 | −209 | −49 | 1549.126 | −238 | −17 | 1567.964 | −241 | −14 | 1587.075 | −225 | 10  |
| 6    | 1530.355 | 245  | 42  | 1549.044 | 249  | 21  | 1567.898 | 266  | −18 | 1586.966 | 219  | 34  |
| 7    | 1530.105 | 310  | 70  | 1548.783 | 329  | 52  | 1567.600 | 337  | 22  | 1586.715 | 276  | 48  |

**Table 2. Hydrogen-loaded sample. Initial FBG wavelength (straight) and wavelength shifts (in pm) after bending (B) and after irradiation (I)**

| Core | FBG 1 Initial | B | I | FBG 2 Initial | B | I | FBG 3 Initial | B | I | FBG 4 Initial | B | I |
|------|---------|------|------|---------|------|------|---------|------|------|---------|------|------|
| 1 | 1531.118 | −169 | −332 | 1549.871 | −170 | −321 | 1568.609 | −151 | −317 | 1587.351 | −106 | −325 |
| 2 | 1531.287 | 108 | −333 | 1550.048 | 125 | −360 | 1568.838 | 128 | −295 | 1587.570 | 189 | −333 |
| 3 | 1531.121 | 169 | −330 | 1549.886 | 194 | −315 | 1568.698 | 238 | −378 | 1587.412 | 253 | −353 |
| 4 | 1530.942 | −113 | −360 | 1549.676 | −108 | −271 | 1568.405 | −45 | −405 | 1587.172 | −79 | −346 |
| 5 | 1531.092 | −450 | −360 | 1549.846 | −461 | −301 | 1568.600 | −439 | −380 | 1587.363 | −449 | −358 |
| 6 | 1530.978 | −515 | −349 | 1549.726 | −521 | −384 | 1568.476 | −539 | −340 | 1587.231 | −492 | −374 |
| 7 | 1531.224 | −241 | −386 | 1549.987 | −238 | −415 | 1568.767 | −270 | −297 | 1587.513 | −193 | −362 |

In optical fiber sensors based on MCFs, the measurement can be encoded in the differences between cores. For shape sensors, curvature, $\kappa$, curvature radius, $r$, and curvature direction, $\theta$, can be determined using the following equations,

$$\vec{\kappa}_{app} = -\sum_{i=2}^{7} \frac{\varepsilon_i}{d} \cos\left(\frac{\pi}{3}(i-1)\right)\hat{j} - \sum_{i=2}^{7} \frac{\varepsilon_i}{d} \sin\left(\frac{\pi}{3}(i-1)\right)\hat{k} , \tag{1}$$

$$\varepsilon_i = \frac{\Delta\lambda_i}{k_i} , \tag{2}$$

$$\kappa = \frac{|\vec{\kappa}_{app}|}{3} , \tag{3}$$

$$r = \frac{1}{\kappa} , \tag{4}$$

$$\theta = \tan^{-1}\left(\frac{\kappa_{app,\hat{k}}}{\kappa_{app,\hat{j}}}\right) + \phi \text{ where } \phi = \begin{cases} 0 & \kappa_{app,\hat{j}} \leq 0 \\ \pi & \kappa_{app,\hat{j}} > 0 \end{cases} , \tag{5}$$

where $\varepsilon_i$, are the strain values in external cores, $\Delta\lambda_i$ is the wavelength shift measured in each core, $k_i$ is the strain sensitivity and $d$ is the distance of the external cores to the fiber center [17]. For convenience, the $\hat{j}$ axis is selected to point core #2 and coefficient $\phi$ is used for angle disambiguation. The MCF used is homogeneous and all the cores have the same strain sensitivity and are at the same distance to the fiber center but this is not a requirement.

Deriving the summations in [Eq. (1)] one can observe that the signs of cosines and sines are opposed for cores 2 and 5, 3 and 6, and 4 and 7. A wavelength shift common to all the cores is then subtracted, making the sensor immune to the RI-BWS.

We have calculated the curvature radius and direction for every FBG before and after the irradiation. Figure 6 shows the obtained values in each position along the optical fiber.

In the unloaded fiber, the mean curvature radius and the mean curvature direction before the irradiation were 20.44 cm and 73.39° respectively whereas after the irradiation of the sample they are 19.38 cm and 77.48°. In the hydrogen-loaded fiber, the mean curvature radius and the mean curvature direction were 20.79 cm and −139.07° whereas after the irradiation the obtained mean values are 20.12 cm and −138.42°. It is worth noting that the differences between the calculated curvature radius and direction before and after the irradiation are similar in both fibers, even if the RI-BWS in the hydrogen-loaded fiber is near ten times higher, demonstrating that the measurement error does not depend on the wavelength shift produced by $\gamma$-radiation. The small curvature errors can be attributed to the manipulation of the fiber and the metallic structure during the experimental test and the Bragg wavelength determination errors [18].
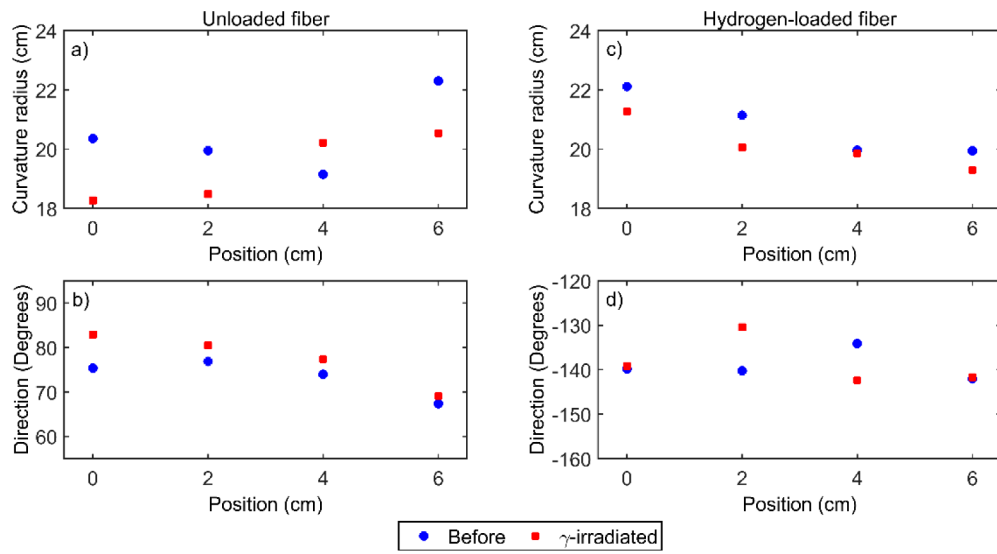
**Fig. 6.** Curvature radius and direction before and after the irradiation. Unloaded fiber (a) and (b) and hydrogen-loaded fiber (c) and (d).

## 5. Conclusions

We have implemented a fiber optic shape sensor, tolerant to high-energy ionizing environments. It is hardened by design, based on FBGs inscribed in the cores of an MCF and using the sensitivity differences of the cores. We have experimentally demonstrated the immunity of these sensors implementing two shape sensors in hydrogen-loaded and unloaded fibers to have different radiation sensitivities. The two samples were coiled in a metallic structure and exposed to a $^{60}$Co radioactive source, up to 0.19 MGy. As expected, after the fiber irradiation, the hydrogen-loaded fiber shows a higher wavelength shift that is about ten times higher than the one observed for the unloaded fiber. However, the differences between the curvature radius and direction before and after the irradiation of the fibers are similar in both samples, demonstrating that the radiation-induced Bragg wavelength shift does not influence the curvature measurement. The same concept can be applied to implement fiber optic sensors for other parameters in high-energy ionizing environments.

## References

1. S. Bandyopadhyay, J. Canning, M. Stevenson, and K. Cook, "Ultrahigh-temperature regenerated gratings in boron-codoped germanosilicate optical fiber using 193 nm," Opt. Lett. **33**(16), 1917–1919 (2008).
2. D. Barrera, V. Finazzi, J. Villatoro, S. Sales, and V. Pruneri, "Packaged Optical Sensors Based on Regenerated Fiber Bragg Gratings for High Temperature Applications," IEEE Sens. J. **12**(1), 107–112 (2012).

3. J.-Y. Huang, J. V. Roosbroeck, J. Vlekken, A. B. Martinez, T. Geernaert, F. Berghmans, B. V. Hoe, E. Lindner, and C. Caucheteur, "FBGs written in specialty fiber for high pressure/high temperature measurement," Opt. Express **25**(15), 17936 (2017).
4. A. Gusarov, F. Berghmans, O. Deparis, A. Fernandez, Y. Defosse, P. Megret, M. Decreton, and M. Blondel, "High total dose radiation effects on temperature sensing fiber Bragg gratings," IEEE Photonics Technol. Lett. **11**(9), 1159–1161 (1999).
5. M. Perry, P. Niewczas, and M. Johnston, "Effects of Neutron-Gamma Radiation on Fiber Bragg Grating Sensors: A Review," IEEE Sens. J. **12**(11), 3248–3257 (2012).
6. S. Girard, A. Morana, A. Ladaci, T. Robin, L. Mescia, J.-J. Bonnefois, M. Boutillier, J. Mekki, A. Paveau, B. Cadier, E. Marin, Y. Ouerdane, and A. Boukenter, "Recent advances in radiation-hardened fiber-based technologies for space applications," J. Opt. **20**(9), 093001 (2018).
7. A. Gusarov and S. K. Hoeffgen, "Radiation Effects on Fiber Gratings," IEEE Trans. Nucl. Sci. **60**(3), 2037–2053 (2013).
8. A. Morana, S. Girard, E. Marin, C. Marcandella, P. Paillet, J. Périsse, J.-R. Macé, A. Boukenter, M. Cannas, and Y. Ouerdane, "Radiation tolerant fiber Bragg gratings for high temperature monitoring at MGy dose levels," Opt. Lett. **39**(18), 5313–5316 (2014).
9. A. Morana, S. Girard, E. Marin, M. Lancry, C. Marcandella, P. Paillet, L. Lablonde, T. Robin, R. J. Williams, M. J. Withford, A. Boukenter, and Y. Ouerdane, "Influence of photo-inscription conditions on the radiation-response of fiber Bragg gratings," Opt. Express **23**(7), 8659–8669 (2015).
10. J. Kuhnhenn, U. Weinand, A. Morana, S. Girard, E. Marin, J. Perisse, J. Genot, J. Grelin, G. Melin, B. Cadier, T. Robin, J.-R. Mace, A. Boukenter, and Y. Ouerdane, "Gamma Radiation Tests of Radiation-Hardened Fiber Bragg Grating Based Sensors for Radiation Environments," IEEE Trans. Nucl. Sci. **64**(8), 2307–2311 (2017).
11. A. Gusarov, F. Berghmans, A. Fernandez, O. Deparis, Y. Defosse, D. Starodubov, M. Decreton, P. Megret, and M. Bondel, "Behavior of fibre Bragg gratings under high total dose gamma radiation," IEEE Trans. Nucl. Sci. **47**(3), 688–692 (2000).
12. D. Barrera, J. Hervás, I. Gasulla, and S. Sales, "Enhanced accuracy sensors using multicore optical fibres based on RFBGs for temperatures up to 1000°C," Proc. SPIE **9916**, 99161J (2016).
13. G. M. H. Flockhart, W. N. Macpherson, J. S. Barton, J. D. C. Jones, L. Zhang, and I. Bennion, "Two-axis bend measurement with Bragg gratings in multicore optical fiber," Opt. Lett. **28**(6), 387–389 (2003).
14. D. Barrera, I. Gasulla, and S. Sales, "Multipoint Two-Dimensional Curvature Optical Fiber Sensor Based on a Nontwisted Homogeneous Four-Core Fiber," J. Lightwave Technol. **33**(12), 2445–2450 (2015).
15. T. Blanchet, A. Morana, G. Laffont, R. Cotillard, E. Marin, A. Boukenter, Y. Ouerdane, and S. Girard, "Radiation Effects on Type I Fiber Bragg Gratings: Influence of Recoating and Irradiation Conditions," J. Lightwave Technol. **36**(4), 998–1004 (2018).
16. D. Tosi, "Review and Analysis of Peak Tracking Techniques for Fiber Bragg Grating Sensors," Sensors **17**(10), 2368 (2017).
17. J. P. Moore and M. D. Rogge, "Shape sensing using multi-core fiber optic cable and parametric curve solutions," Opt. Express **20**(3), 2967–2973 (2012).
18. I. Floris, S. Sales, P. A. Calderón, and J. M. Adam, "Measurement uncertainty of multicore optical fiber sensors used to sense curvature and bending direction," Measurement **132**, 35–46 (2019).